

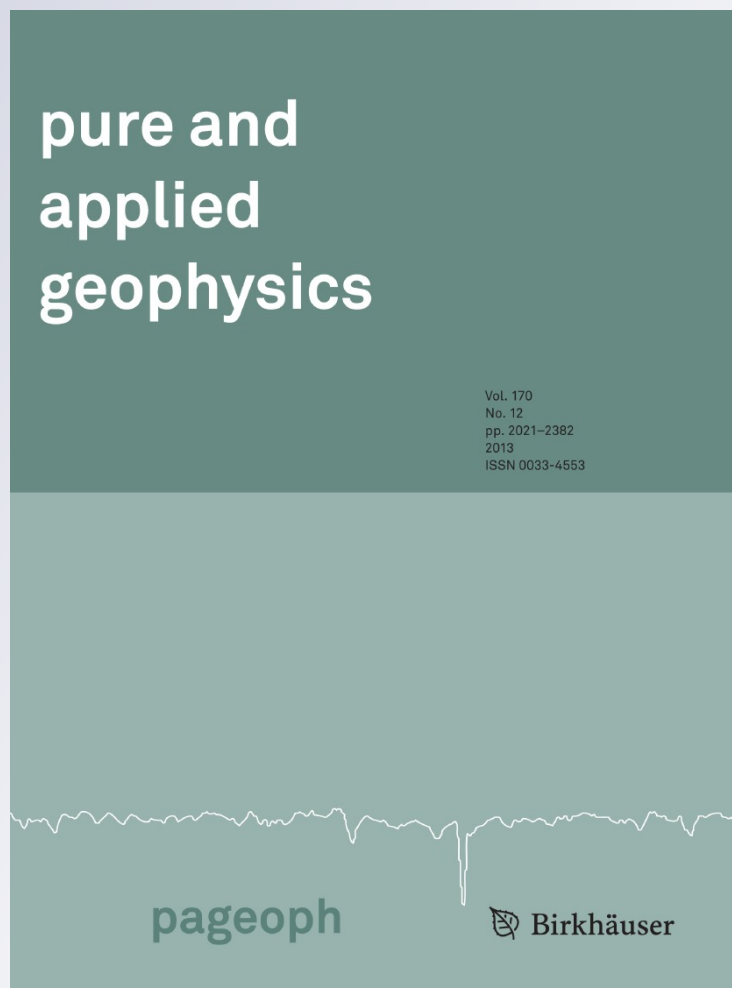
Seismic Rheological Model and Reflection Coefficients of the Brittle–Ductile Transition

José M. Carcione & Flavio Poletto

Pure and Applied Geophysics
pageoph

ISSN 0033-4553
Volume 170
Number 12

Pure Appl. Geophys. (2013)
170:2021–2035
DOI 10.1007/s00024-013-0643-4



Your article is protected by copyright and all rights are held exclusively by Springer Basel. This e-offprint is for personal use only and shall not be self-archived in electronic repositories. If you wish to self-archive your article, please use the accepted manuscript version for posting on your own website. You may further deposit the accepted manuscript version in any repository, provided it is only made publicly available 12 months after official publication or later and provided acknowledgement is given to the original source of publication and a link is inserted to the published article on Springer's website. The link must be accompanied by the following text: "The final publication is available at link.springer.com".

Seismic Rheological Model and Reflection Coefficients of the Brittle–Ductile Transition

JOSÉ M. CARCIONE¹ and FLAVIO POLETTI¹

Abstract—It is well established that the upper—cooler—part of the crust is brittle, while deeper zones present ductile behaviour. In some cases, this brittle–ductile transition is a single seismic reflector with an associated reflection coefficient. We first develop a stress–strain relation including the effects of crust anisotropy, seismic attenuation and ductility in which deformation takes place by shear plastic flow. Viscoelastic anisotropy is based on the eigenstrain model and the Zener and Burgers mechanical models are used to model the effects of seismic attenuation, velocity dispersion, and steady-state creep flow, respectively. The stiffness components of the brittle and ductile media depend on stress and temperature through the shear viscosity, which is obtained by the Arrhenius equation and the octahedral stress criterion. The P- and S-wave velocities decrease as depth and temperature increase due to the geothermal gradient, an effect which is more pronounced for shear waves. We then obtain the reflection and transmission coefficients of a single brittle–ductile interface and of a ductile thin layer. The PP scattering coefficient has a Brewster angle (a sign change) in both cases, and there is substantial PS conversion at intermediate angles. The PP coefficient is sensitive to the layer thickness, unlike the SS coefficient. Thick layers have a well-defined Brewster angle and show higher reflection amplitudes. Finally, we compute synthetic seismograms in a homogeneous medium as a function of temperature.

Key words: Brittle–ductile transition, melting, anisotropy, attenuation, shear flow, reflection coefficient.

1. Introduction

The brittle–ductile transition (BDT) plays an important role in earthquake seismology and geothermal studies (CARTER and KIRBY, 1978; MEISSNER and STREHLAU, 1982; BATINI and NICOLICH, 1985; HOBBS *et al.*, 1986; CAMELI *et al.*, 1993; VERGNOLLE *et al.*, 2003; MATTEIS *et al.*, 2008; DOGLIONI *et al.*, 2011). The BDT may be one of the factors that

control plate-tectonic activity such as the generation of mountains and plate break-up. Moreover, it may be the cause that triggers large shallow earthquakes, following the conclusions of MEISSNER and STREHLAU (1982) who found that the brittle–ductile yield stress envelope has the same form of the frequency–depth distribution, with a peak in the upper and middle crust. Measurements and models reveal that below this interface, determined by pressure–temperature conditions, aseismic slip activity dominates, since earthquakes cannot be sustained in ductile layers. The nucleation of earthquakes occurs in the upper brittle part, since large deviatoric stresses cannot be generated for long periods of time in such ductile media. A possible scenario is shown in Fig. 1, where a thin layer and a single interface can generate a significant reflection event.

CAMELI *et al.* (1993) claim that at the Larderello geothermal field the so-called K horizon represents the boundary separating the brittle and the ductile crust. They state that excess temperature below the geothermal area induces a ductile behaviour, and that earthquakes nucleate at the K horizon. The K horizon in central Italy has been taken by CARCIONE *et al.* (2003) as a major interface overlying the top of the lower crust, the Moho of the Adria plate, the top of the subducted slab of the Alpine Tethys, and the Moho of the subducted Tethyan slab. Generally, it is widely accepted that the crust can roughly be modeled with an upper brittle layer and a lower ductile layer (RUTTER 1986). More evidence indicates that the K horizon in the upper crust corresponds to a shear plane separating the brittle crust from the ductile crust (BROGI *et al.*, 2003; LIOTTA and RANALLI, 1999).

The viscosity of the crust is a fundamental factor in defining the properties of the BDT interface, since it is controlled by the geothermal temperature. The viscosity ranges from about 10^{25} Pa s in a cold brittle

¹ OGS, Istituto Nazionale di Oceanografia e di Geofisica Sperimentale, Borgo Grotta Gigante 42c, 34010 Sgonico, Trieste, Italy. E-mail: jcarcione@inogs.it

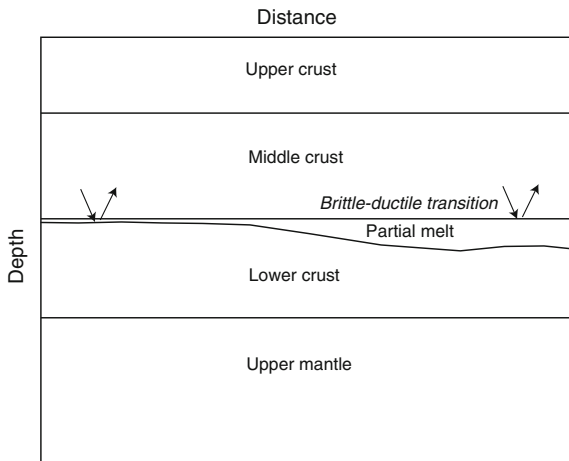


Figure 1

Scheme of the Earth's crust showing possible scenarios of the brittle-ductile transition, namely, reflection from a thin layer (left) and a reflection from a single interface (right)

crust, down to about 10^{18} Pa s in the ductile, more hot, crust. The wave-velocity contrast is mainly due to the dissimilar shear rigidity, with much lower values in the ductile medium (MATSUMOTO and HASEGAWA, 1996). The ductile medium mainly flows when subjected to distortional or deviatoric stress. Under isotropic stress (often called hydrostatic stress), this medium does not flow appreciably even though it will deform elastically (small strains or deformations). It flows under isotropic stress to achieve (minor) porosity reduction. The magnitude of the deviatoric stress is proportional to the octahedral stress, a scalar that is invariant under coordinate transformations and whose value determines the character of the flow.

There is experimental evidence that linear viscoelastic models are appropriate to describe the behavior of ductile media. GANGI (1981, 1983), among others, obtained exponential functions of time using linear viscoelastic models to fit data for synthetic and natural rocksalt. The viscoelastic creep—with steady-state creep—of salt has been described by a Burgers model which includes the transient creep of the Zener model, which does not exhibit steady-state creep, and the steady-state creep of a Maxwell model (CARCIONE *et al.*, 2006). On the other hand, CHAUVEAU and KAMINSKI (2008) described the effect of transient creep on the compaction process on the basis of a Burgers's model. The Burgers model is

shown in Fig. 2 (the Maxwell and Zener models are particular cases of the Burgers model). Comprehensive reviews and the mathematical basis for describing the Burgers rheology can be found in MAINARDI (2010) and MAINARDI and SPADA (2011). Here, the Zener model is used to model the viscoelastic deformation with no plastic flow. The type of viscoelastic model depends on the value of the octahedral stress, which determines the limit separating transient flow from unrecoverable steady-state flow. The nature of seismic attenuation as well steady-state viscosity effects can be explained with the dislocation theory, where the relaxation times depend on the in-situ stress and temperature conditions (ANDERSON, 1989). Alternative models were developed by WALSH (1969) where the liquid phase are lens-shaped inclusions of melt or films of melt surrounding spherical grains. A relatively new, porous model, that could possibly contribute to damp seismic waves is the mesoscopic-loss mechanism, by which wave energy is converted to diffusion energy of the Biot slow-mode type (e.g., CARCIONE and PICOTTI, 2006).

Seismic wave propagation is described by the eigenstrain theory (CARCIONE and CAVALLINI, 1994; CARCIONE, 2007) to model anisotropy and attenuation in the crust, while the Burgers model is used to model the ductility effects (CARCIONE *et al.*, 2006). The crust is then described by a transversely isotropic stress-strain

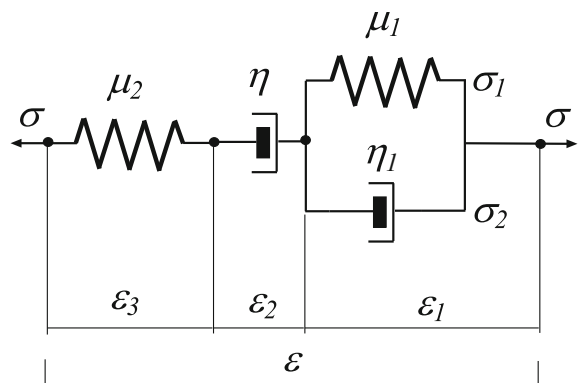


Figure 2

Mechanical representation of the Burgers viscoelastic model for shear deformations (e.g., CARCIONE, 2007). σ , ϵ , μ , and η represent stress, strain, shear modulus, and viscosity, respectively, where η_1 (Zener viscosity) describes seismic relaxation, while η (Burgers viscosity) is related to plastic flow and processes such as dislocation creep

relation with five (independent) complex and frequency dependent stiffnesses. The type of creep is regulated by critical octahedral-stress values and a flow viscosity as a function of temperature and pressure. Next, we obtain the reflection and transmission coefficients of the BDT, represented as a single interface. The theory can be found in CARCIONE (1997, 2007) and SIDLER *et al.* (2008).

Finally, we compute synthetic seismograms in homogeneous media to study the effects of temperature on the attributes of the seismic wavefield, particularly, attenuation and velocity dispersion. One feasible and economic technique to measure the seismic properties is seismic while drilling, a method that exploits the drill-bit noise as a source of seismic waves (POLETTO and MIRANDA, 2004). This technique has been adapted for geophysical exploration in geothermal wells (POLETTO *et al.*, 2011).

2. Mean and Octahedral Stresses

We use the octahedral-stress theory to describe the deformation of the ductile layer. In Cartesian coordinates (x, y, z) , we define the octahedral stress as

$$\tau_o = \frac{1}{3} \sqrt{(\sigma_v - \sigma_h)^2 + (\sigma_v - \sigma_H)^2 + (\sigma_h - \sigma_H)^2}, \tag{1}$$

where the σ 's are the stress components in the principal system, corresponding to the vertical (v) lithostatic stress, and the maximum (H) and minimum (h) horizontal tectonic stresses (see Fig. 3a). Figure 3b shows the octahedral stress as a function of the octahedral strain. When the stress vector associated with the normal to the octahedral plane is generated, its components in the principal directions are the eigenstresses (or principal stresses). Alternatively, it has two components—one normal to the plane (which has a magnitude equal to the mean stress) and one tangential to the plane which has a magnitude equal to the octahedral stress (the latter is proportional to the magnitude of the deviatoric stress).

The rock starts to yield when τ_o exceeds the elastic octahedral-stress limit τ_{oe} . Below this limit, there is gradual creep deformation when constant

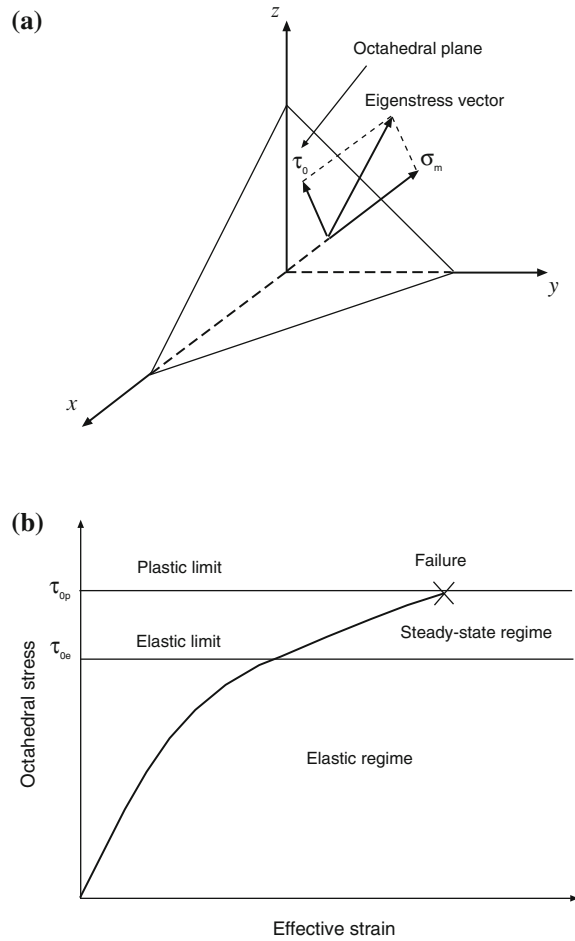


Figure 3

Mean and octahedral stresses (a) versus octahedral (effective) strain (b). The octahedral-stress vector, which is a measure of the shear deformation, lies on the octahedral plane. The normal to this surface makes the same angle with the direction of the three principal stresses σ_v , σ_h and σ_H ($\sigma_m = (\sigma_v + \sigma_h + \sigma_H)/3$ is the mean stress)

stress is applied. Then, if τ_o is lower than the elastic limit τ_{oe} , the material follows a viscoelastic stress–strain relation. If τ_o lies between τ_{oe} and the plastic limit τ_{op} , steady-state flow occurs. Beyond τ_{op} failure is likely to occur.

3. Stress–Strain Relations

The constitutive equation including both the viscoelastic and ductile behaviour, can be written as a

generalization of the one-dimensional (1D) stress–strain relation reported by DRAGONI (1990) and DRAGONI and PONDRELLI (1991) to the three-dimensional (3D) anisotropic and anelastic case, replacing the Maxwell model by the Burgers model and using the eigenstrain theory introduced by CARCIONE and CAVALLINI (1994) (see also CARCIONE *et al.*, 2006; CARCIONE, 2007). In the frequency-domain and using the Voigt notation, we have

$$\boldsymbol{\sigma} = \mathbf{P} \cdot \mathbf{e}, \quad (2)$$

where

$$\boldsymbol{\sigma} = [\sigma_{11}, \sigma_{22}, \sigma_{33}, \sigma_{23}, \sigma_{13}, \sigma_{12}]^T \quad (3)$$

is the stress vector,

$$\mathbf{e} = [\epsilon_{11}, \epsilon_{22}, \epsilon_{33}, 2\epsilon_{23}, 2\epsilon_{13}, 2\epsilon_{12}]^T, \quad (4)$$

is the strain vector and \mathbf{P} is the stiffness matrix whose components are given below. The stress and strain components σ_{ij} and ϵ_{ij} correspond to the standard notation in 3D space (e.g., CARCIONE, 2007).

For a transversely isotropic medium with unrelaxed elasticity constants c_{IJ} , the complex stiffness components are

$$\begin{aligned} p_{11} &= \Lambda_1(2 + a^2)^{-1} + \Lambda_2(2 + b^2)^{-1} + \Lambda_4/2 \\ p_{12} &= p_{11} - \Lambda_4 \\ p_{33} &= a^2\Lambda_1(2 + a^2)^{-1} + b^2\Lambda_2(2 + b^2)^{-1} \\ p_{13} &= a\Lambda_1(2 + a^2)^{-1} + b\Lambda_2(2 + b^2)^{-1} \\ p_{55} &= \Lambda_3/2 \\ p_{66} &= \Lambda_4/2, \end{aligned} \quad (5)$$

where

$$\begin{aligned} a &= \frac{4c_{13}}{c_{11} + c_{12} - c_{33} + \sqrt{c}}, \\ b &= \frac{4c_{13}}{c_{11} + c_{12} - c_{33} - \sqrt{c}}, \end{aligned} \quad (6)$$

and $\Lambda_I(\omega)$, $I = 1, \dots, 4$ are complex and frequency-dependent eigenstiffnesses, given by

$$\begin{aligned} \Lambda_1 &= \frac{1}{2}(c_{11} + c_{12} + c_{33} + \sqrt{c})M_1 \\ \Lambda_2 &= \frac{1}{2}(c_{11} + c_{12} + c_{33} - \sqrt{c})M_2 \\ \Lambda_3 &= 2c_{55}M_2 \\ \Lambda_4 &= (c_{11} - c_{12})M_2, \end{aligned} \quad (7)$$

with

$$c = 8c_{13}^2 + (c_{11} + c_{12} - c_{33})^2, \quad (8)$$

where

$$M_1 = \frac{1 + i\omega\tau_\epsilon^{(1)}}{1 + i\omega\tau_\sigma^{(1)}} \quad (9)$$

is a Zener (dilatational) kernel, ω is the angular frequency, with $i = \sqrt{-1}$, and

$$M_2 = \frac{1 + i\omega\tau_\epsilon^{(2)}}{1 + i\omega\tau_\sigma^{(2)} - \frac{i\mu}{\omega\eta}(1 + i\omega\tau_\epsilon^{(2)})} \quad (10)$$

is a Burgers (shear) kernel (CARCIONE, 2007). The quantities τ_σ and τ_ϵ are seismic relaxation times,

$$\mu = \frac{1}{6}(4c_{55} + c_{11} - c_{12}), \quad (11)$$

and η is the flow viscosity describing the ductile behaviour related to shear deformations. Evidence of a single relaxation peak in partially melted rocks is discussed by SATO (2005). The theory can easily be generalized to more relaxation mechanisms by adding Zener elements in a series or a parallel connection (e.g., CARCIONE, 2007). The use of more elements depends on the availability of experimental data at different frequency ranges.

The relaxation times can be expressed as

$$\begin{aligned} \tau_\epsilon^{(m)} &= \frac{\tau_0}{Q_0^{(m)}} \left(\sqrt{Q_0^{(m)2} + 1} + 1 \right), \\ \tau_\sigma^{(m)} &= \tau_\epsilon^{(m)} - \frac{2\tau_0}{Q_0^{(m)}}, \\ m &= 1, 2, \end{aligned} \quad (12)$$

where τ_0 is a relaxation time such that $\omega_0 = 1/\tau_0$ is the center frequency of the relaxation peak and $Q_0^{(m)}$ are the minimum quality factors.

The twofold eigenstiffnesses Λ_3 and Λ_4 are related to pure “isochoric” eigenstrains, i.e., to volume-preserving changes of shape only, while the single eigenstiffnesses Λ_1 and Λ_2 are related to eigenstrains that consist of simultaneous changes in volume and shape. For relatively weak anisotropy, Λ_1 corresponds to a quasi-dilatational deformation and Λ_2 to a quasi-shear deformation. Moreover, Λ_3 and Λ_4 determine the mechanical behaviour of the shear waves along the principal axes. According to these

arguments and Eqs. (9) and (10), the ductile medium shows permanent relaxation of the normal and shear stresses.

The limit $\eta \rightarrow \infty$ in Eq. (10) recovers the Zener kernel to describe the behaviour of the brittle material, while $\tau_\sigma^{(2)} \rightarrow 0$ and $\tau_\epsilon^{(2)} \rightarrow 0$ (or, more generally, $\tau_\sigma^{(2)} = \tau_\epsilon^{(2)}$) yield the Maxwell model used by DRAGONI (1990) and DRAGONI and PONDRELLI (1991):

$$M_2 = \left(1 - \frac{i\mu}{\omega\eta}\right)^{-1} \quad (13)$$

(e.g., CARCIONE, 2007). For $\eta \rightarrow 0$, $M_2 \rightarrow 0$ and the medium becomes an anisotropic fluid whose anelastic properties are governed by the kernel M_1 , with $p_{33} = a^2 p_{11}$, $p_{12} = p_{11}$ and $p_{13} = ap_{11}$.

The viscosity η can be expressed by the Arrhenius equation (e.g., CARCIONE *et al.*, 2006). It is related to the steady-state creep rate $\dot{\epsilon}$ by

$$\eta = \frac{\tau_o}{2\dot{\epsilon}}, \quad (14)$$

where τ_o is the octahedral stress. It can be expressed as

$$\dot{\epsilon} = A_\infty \tau_o^n \exp(-E/RT) \quad (15)$$

(e.g., GANGI, 1983; CARCIONE *et al.*, 2006), where A_∞ and n are constants, E is the activation energy, $R = 8.3144$ J/mol/K is the gas constant and T is the absolute temperature. The form of the empirical relation (15) is determined by performing experiments at different strain rates, temperatures and/or stresses (e.g., GANGI, 1983; CARTER and HANSEN, 1983).

4. Reflection and Refraction Coefficients

The coefficients for a single interface and a layer can be found in CARCIONE (1997, 2007). For an incident wave with subscript $W = P$ or $W = S$, where P and S denote compressional and shear waves, the reflection-transmission coefficient vector is

$$[R_{WP}, R_{WS}, T_{WP}, T_{WS}]^\top = (\mathbf{B}\mathbf{A}_2 - \mathbf{A}_1)^{-1} \mathbf{i}_W, \quad (16)$$

where \mathbf{A}_1 and \mathbf{A}_2 are the propagator matrices related to the upper and lower media, \mathbf{B} is the propagator matrix of the layer, and \mathbf{i}_W is the incidence vector. The explicit expressions can be found in CARCIONE (2007) (Chapter 6). This approach, which is the basis

of most reflectivity methods, dates back to THOMSON (1950). For a layer with zero thickness, we obtain the coefficients of a single interface.

5. Synthetic Pulses

We compute transient seismic waves in homogeneous media by superposing plane waves and performing a numerical integration from the frequency to the time domain. The field at distance x , initiated by a source whose spectrum is $S(\omega)$, is given by

$$u(x, t) = \text{Re} \int S(\omega) \exp[i(\omega t - \kappa x)] \exp(-\alpha x) d\omega, \quad (17)$$

where $\kappa(\omega)$ is the wavenumber, $\alpha(\omega)$,

$$\alpha(\omega) = \frac{\pi f}{Q(\omega)v(\omega)} \quad (18)$$

is the attenuation factor, where $f = \omega/(2\pi)$ is the frequency and $v(\omega)$ is the phase velocity. The definition of these kinematic quantities can be found, for instance, in CARCIONE (2007).

6. Example

The brittle and ductile rocks are described by the same unrelaxed properties, with the following Thomsen parameters: $\epsilon = 0.05$, $\gamma = 0.1$ and $\delta = 0.2$, and a vertical P-wave velocity $v_{33} = 6$ km/s (CHEN *et al.*, 2009; VAVRYČUK, 2005). Assuming a Poisson medium, we obtain the vertical S-wave velocity as $v_{55} = v_{33}/\sqrt{3}$. Then, $c_{33} = \rho v_{33}^2$, where $\rho = 2,600$ kg/m³, $c_{11} = c_{33}(1 + 2\epsilon)$, $c_{66} = c_{55}(1 + 2\gamma)$ and $c_{13} = \sqrt{2\delta c_{33}(c_{33} - c_{55}) + (c_{33} - c_{55})^2} - c_{55}$. The density is assumed constant as a first approximation. Stress and temperature increase with depth, and while higher temperatures expand the melts, implying lower density, higher stresses cause melts to compress, implying higher density. Hence, the two effects compensate.

The loss parameters of the brittle and ductile layers are obtained from empirical equations derived

by CASTRO *et al.* (2008) for the crust in southern Italy. They obtain $Q_0^{(2)} = 18.8 f^{1.7}$ for the upper crust and up to a frequency of 10 Hz. We calculate the dilatational Q -factor as $Q_0^{(1)} = Q_0^{(2)}k/\mu$, where μ is given in Eq. (11) and k is a bulk modulus given by

$$k = \frac{1}{9}(6c_{11} + 3c_{33} - 8c_{55} - 4c_{66}).$$

This relation implies that the harder the medium the higher the Q factor, i.e., less attenuation. Moreover, in most of the examples we consider a frequency of $f = 3$ Hz and $\omega_0 = 2\pi f$.

The temperature is a function of depth through the geothermal gradient G as $T = zG$, where z is depth and $G = 60$ °C/km in our calculations. The lithostatic stress is $\sigma_v = \bar{\rho}gz$, where $\bar{\rho} = 2,400$ kg/m³ is the average density and $g = 9.81$ m/s² is the gravity constant. To obtain the octahedral stress (1) we consider a simple model based on the gravity contribution at depth z . The horizontal stresses can be estimated as

$$\sigma_H = \frac{v\sigma_v}{1-v}, \quad \text{and} \quad \sigma_h = \xi\sigma_H \quad (19)$$

where

$$v = \frac{c_{13}(c_{11} - c_{12})}{c_{11}c_{33} - c_{13}^2}, \quad (20)$$

is the Poisson ratio along the horizontal direction (e.g., CARCIONE and CAVALLINI, 2002). The factor $v/(1-v)$ lies between 0.25 and 1 for v ranging from 0.2 to 0.5, with the latter value corresponding to a liquid (hydrostatic stress). The parameter $\xi \leq 1$ has been introduced to model additional effects due to tectonic activity (anisotropic tectonic stress). Furthermore, we consider $A_\infty = 10^{10.8}(\text{MPa})^{-n}\text{s}^{-1}$, $E = 134$ kJ/mol and $n = 2.6$, which correspond to quartzite (KIRBY and KRONENBERG 1987; Table 3, line 11) and take $\xi = 0.8$. The above degree of stress anisotropy is consistent with values at prospective depths provided by HEGRET (1987) for the Canadian Shield, and in agreement with data reported in ENGELDER (1993, p. 91).

The octahedral stress and flow viscosity as a function of depth and temperature are shown in Fig. 4. Let

$$v_{II} = \text{Re}^{-1}\left(\sqrt{\frac{\rho}{p_{II}}}\right) \quad \text{and} \quad Q_{II} = \frac{\text{Re}(p_{II})}{\text{Im}(p_{II})}, \quad (21)$$

$I = 1, 3, 5, 6$

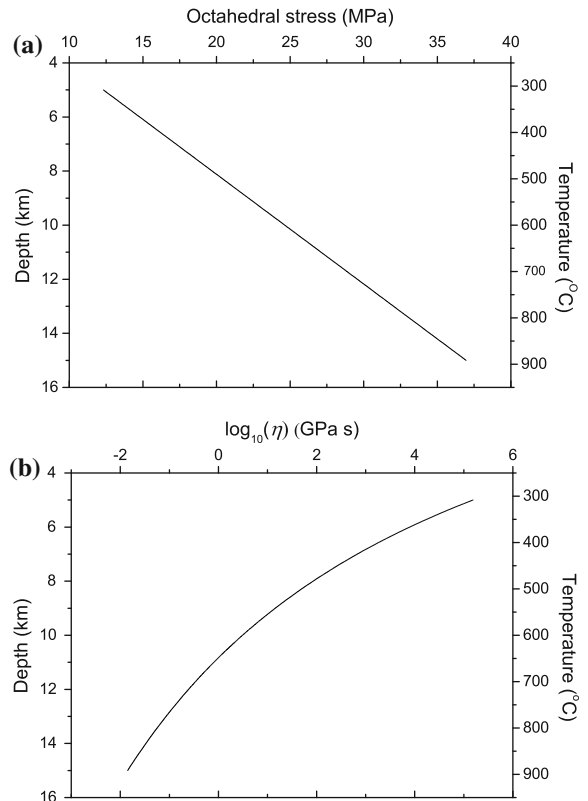


Figure 4
Octahedral stress (a) and flow viscosity (b) as a function of depth and temperature

be the phase velocities and quality factors along the principal axes of the transversely isotropic medium, where “Re” and “Im” denote real and imaginary parts, respectively (e.g., CARCIONE, 2007). The phase velocity, as given in Eq. (21), can also be expressed in terms of the wavenumber κ as ω/κ .

Minimum Q values as a function of the Burgers viscosity can be obtained with good approximation. If we consider that $\tau_\sigma^{(m)} = \tau_\epsilon^{(m)}$, there is no seismic loss and the attenuation is solely due to the Burgers viscosity. We obtain the minimum value of Q_{33} as a function of this viscosity as

$$\bar{Q}_{33} = q_1\bar{\eta} + \frac{q_2}{\bar{\eta}} = \frac{2}{N}\sqrt{K(K+N)},$$

$$\bar{\eta} = \sqrt{\frac{q_2}{q_1}} = \frac{\mu}{\omega}\sqrt{\frac{1}{1+N/K}}, \quad (22)$$

where $\bar{\eta}$ is the critical viscosity,

$$\begin{aligned}
 q_1 &= \frac{\omega}{\mu} \left(\frac{K}{N} + 1 \right), \\
 q_2 &= \frac{\mu K}{\omega N}, \\
 K &= \frac{1}{2} a^2 (2 + a^2)^{-1} (c_{11} + c_{12} + c_{33} + \sqrt{c}), \\
 N &= \frac{1}{2} b^2 (2 + b^2)^{-1} (c_{11} + c_{12} + c_{33} - \sqrt{c}).
 \end{aligned}
 \tag{23}$$

As can be seen, the minimum quality factor depends only on the elastic properties of the medium, while the critical viscosity depends also on frequency. In the isotropic case, we have $a = 1, b = -2, K = k, N = (4/3)\mu, \bar{\eta} = (\mu/\omega)/\sqrt{1 + 4\mu/(3k)}, \bar{Q} = \sqrt{3k(3k + 4\mu)}/(2\mu)$. If the medium is a Poisson solid we obtain $\bar{\eta} = (\mu/\omega)3/\sqrt{5}$ and $\bar{Q} = 3\sqrt{5}/2$. A critical temperature can be defined in terms of the critical viscosity using Eqs. (14) and (15). We obtain

$$\bar{T} (^{\circ}\text{C}) = \frac{E}{R \ln(2A_{\infty} \bar{\eta} \tau_0^{n-1})} - 273,
 \tag{24}$$

where τ_0 and A_{∞} should be given in Pa and $1/(\text{s Pa}^n)$, respectively.

Figure 5 shows the velocities and quality factors as a function of temperature. As can be seen, the P-wave velocities decrease after a given viscosity dictated by a critical (transition) temperature (ca. 900 K) and the Arrhenius equation. The P-wave attenuation has a maximum at this transition and at higher temperatures the medium becomes an anisotropic fluid whose quality factors are solely determined by the kernel M_1 . Indeed, the lack of the shear losses increases the quality factor and the material behaves fluid-like with weaker attenuation. This is consistent with the fact the a pure solid and a pure liquid have weak attenuation and partial saturation (melting in this case) shows lower Q factors, similar to the behaviour of the mesoscopic-loss mechanism (e.g., SINGH *et al.*, 2000; CARCIONE and PICOTTI, 2006). By this mechanism, wave energy is converted to diffusion energy of the Biot slow-mode type, when the heterogeneities of the medium are smaller than the seismic wavelength but greater than a characteristic pore scale.

For instance, the minimum value of Q_{33} is approximately 6 at a critical viscosity of 1.8 GPa s. Evidence of such low Q values in the crust are reported in KAMPFMANN and BERCKHEMER (1985) and

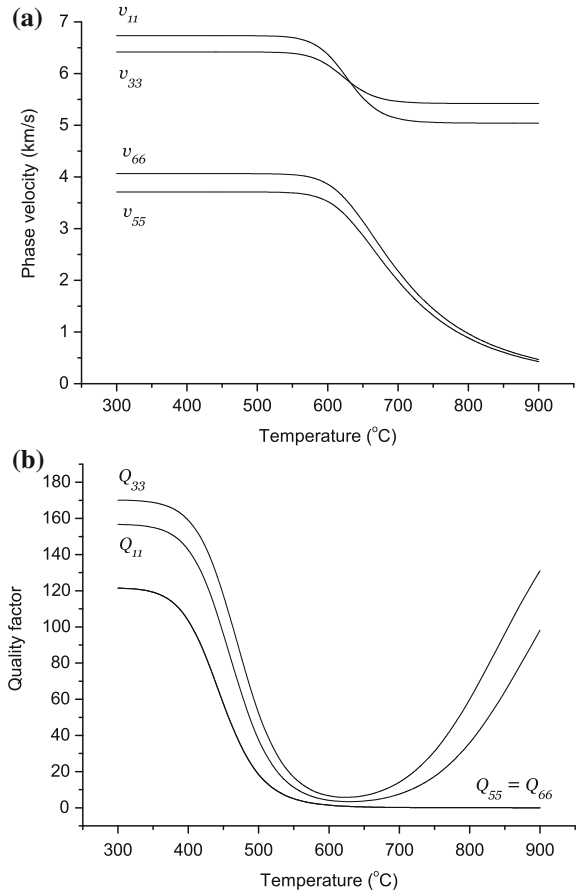


Figure 5

Phase velocities and quality factor along the principal axes of the transversely isotropic medium as a function of temperature. The frequency is 3 Hz

SATO *et al.*, (1988). A good estimation of these critical values can be obtained with Eq. (22).

Appendix shows how to obtain the energy velocities and dissipation factors as a function of the ray and phase angles from the complex stiffnesses (5). Figures 6 and 7 display the energy velocities (a) and quality factors (b) as a function of the ray and propagation (phase) angles for the brittle and ductile medium, with $T = 300$ °C and $T = 700$ °C, respectively. The velocity and attenuation reduction is remarkable in the ductile case, with the shear-wave attenuation Q factors approaching zero. Moreover, the Q_P anisotropy is more pronounced.

Next, we consider seismic frequencies, i.e., $f = 30$ Hz and $\omega_0 = 2\pi f$. However, since the empirical equations for $Q_0^{(2)}$ above holds for frequencies lower

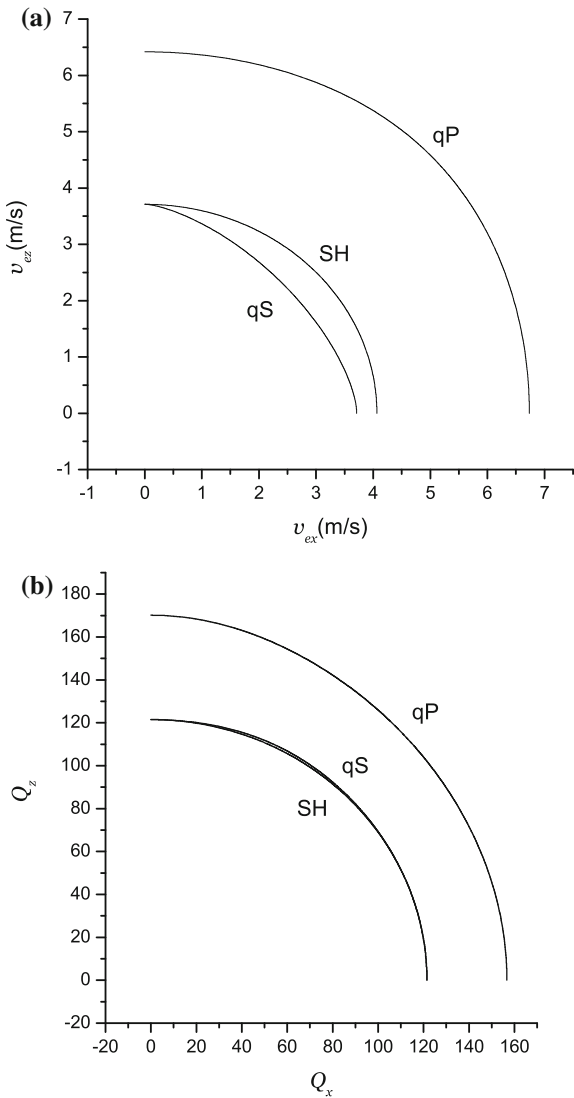


Figure 6

Energy velocities (a) and quality factors (b) as a function of the ray and propagation (phase) angles for the brittle medium ($T = 300\text{ }^\circ\text{C}$). The frequency is 3 Hz

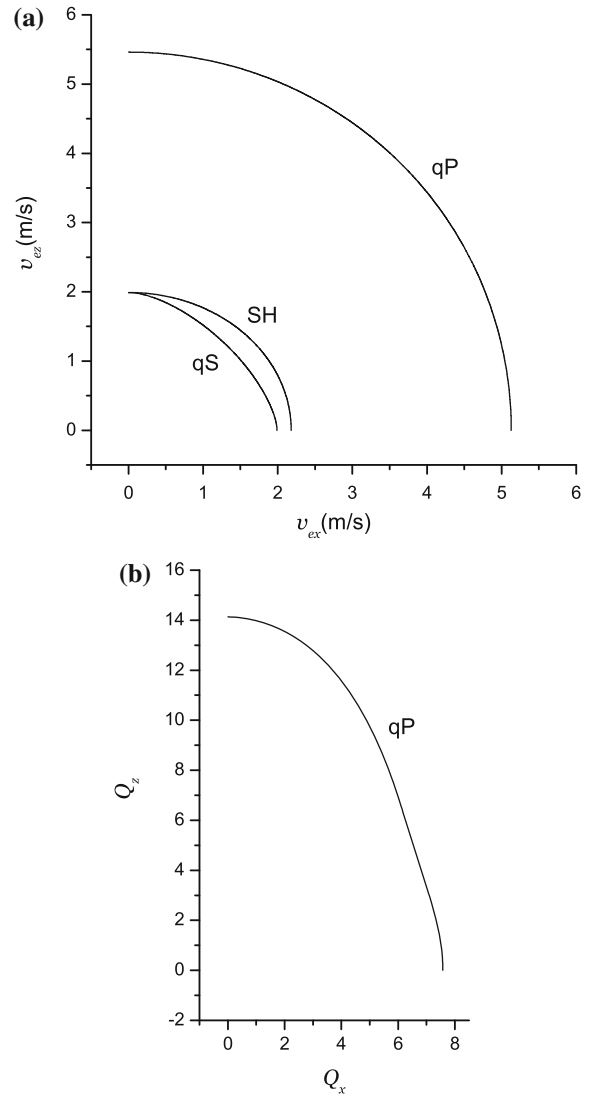


Figure 7

Energy velocities (a) and quality factors (b) as a function of the ray and propagation (phase) angles for the ductile medium ($T = 700\text{ }^\circ\text{C}$). The frequency is 3 Hz

than 10 Hz, we assume the same values of $Q_0^{(1)}$ and $Q_0^{(2)}$ obtained for $f = 3$ Hz. Figure 8 shows the phase velocities and quality factor as a function of temperature. The difference with respect to Fig. 5 are due to the viscosity related to the plastic flow. The transition occurs at higher temperatures ($750\text{ }^\circ\text{C}$ instead of $650\text{ }^\circ\text{C}$) and the P-wave quality factors do not increase significantly after melting.

Figure 9 shows the S to P vertical velocity ratio versus temperature for three frequencies (a) and the

frequency dependence of the quality factors at $718\text{ }^\circ\text{C}$ (b). This ratio, or equivalently the so-called VP/VS ratio, can be an indicator of the presence of fluids or partial melt as can be seen in Fig. 9a, with higher v_{33}/v_{55} values with increasing melting. On the other hand, as Fig. 9b shows, P-wave attenuation is stronger along the horizontal (11) direction. Phase velocity dispersion curves at different temperatures are displayed in Fig. 10. At low temperature, there is no significant dispersion, while at the critical

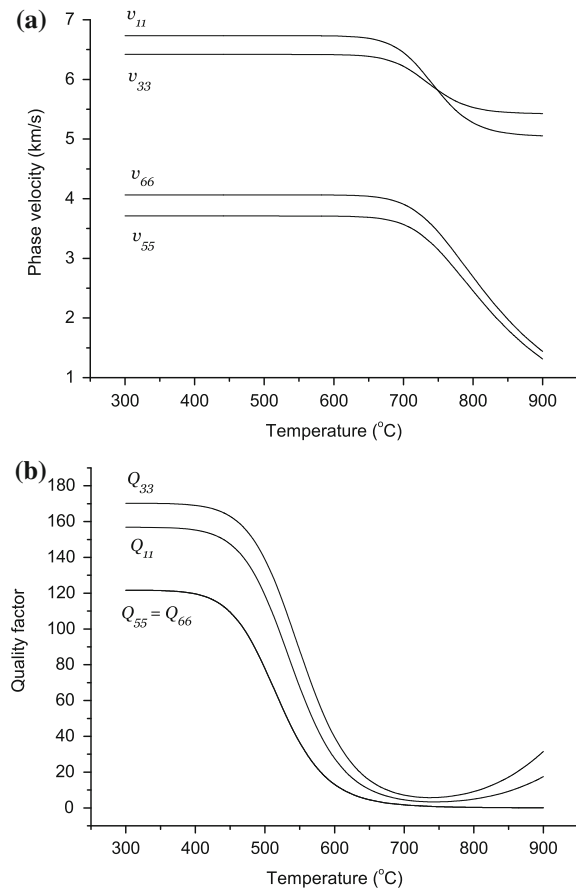


Figure 8

Phase velocities and quality factor along the principal axes of the transversely isotropic medium as a function of temperature. The frequency is 30 Hz

temperature, where partial melt occurs, the dispersion is significant. At higher temperatures, the liquid nature of the rock yields a weaker P-wave dispersion but velocities have opposite behaviour compared to Fig. 10a. Real data to test the theoretical results are scarce or not available. However, laboratory data have been acquired, for instance, by SPETZLER and ANDERSON (1968) who measured the P- and S-wave velocities and attenuation factors in a binary system that is a solid at low temperatures and partially melted at high temperatures. The data indicates that velocities and Q factors drop abruptly at certain critical temperatures and that the low velocity zones show high attenuation values, in qualitative agreement with the results presented here.

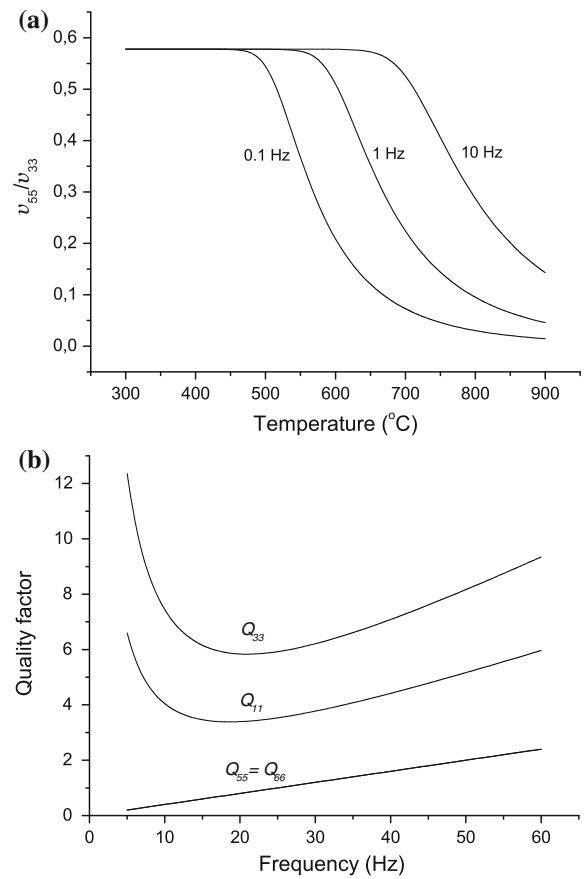


Figure 9

v_{55}/v_{33} ratio versus temperature at three different frequencies (a), and quality factors as a function of frequency corresponding to a temperature of 718 °C (b)

We now compute the reflection and refraction coefficients. First, we consider a single interface separating a brittle medium with stiffnesses

$$\begin{aligned}
 p_{11} &= (122, 0.78) \text{ GPa} \\
 p_{12} &= (33, 0.05) \text{ GPa} \\
 p_{13} &= (57, 0.22) \text{ GPa} \\
 p_{33} &= (111, 0.65) \text{ GPa} \\
 p_{55} &= (37, 0.30) \text{ GPa} \\
 p_{66} &= (45, 0.37) \text{ GPa},
 \end{aligned}$$

corresponding to 300 °C, and a ductile medium defined by

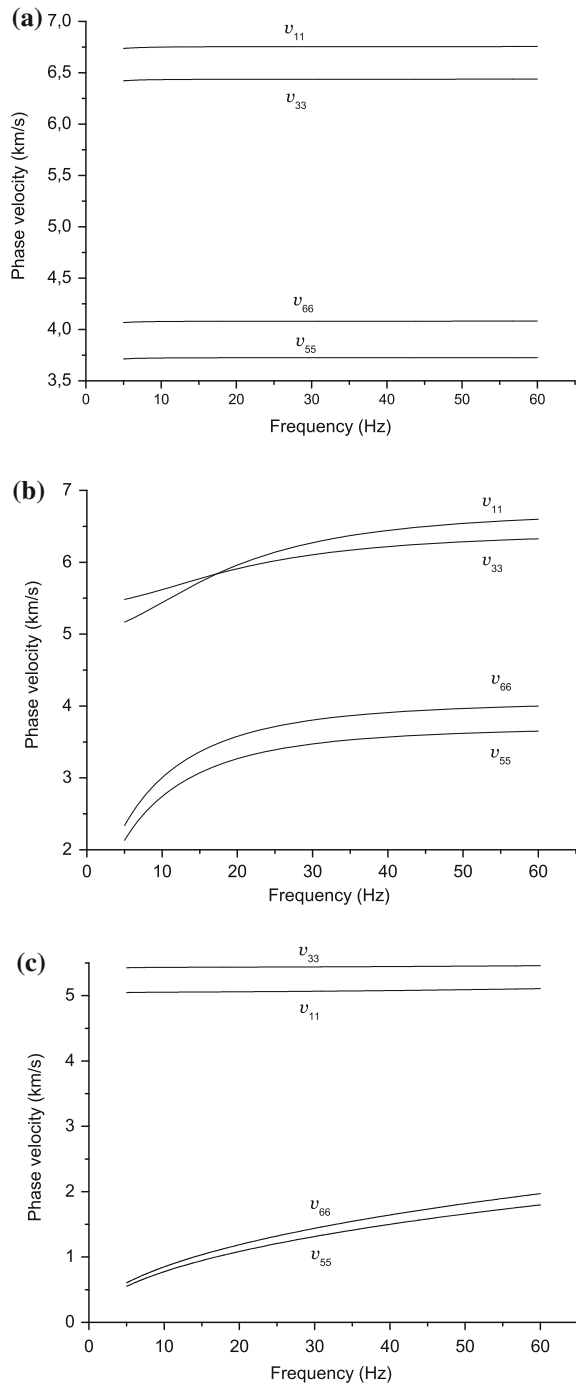


Figure 10

Phase velocity as a function of frequency at 536 °C (a), 718 °C (b) and 900 °C (c)

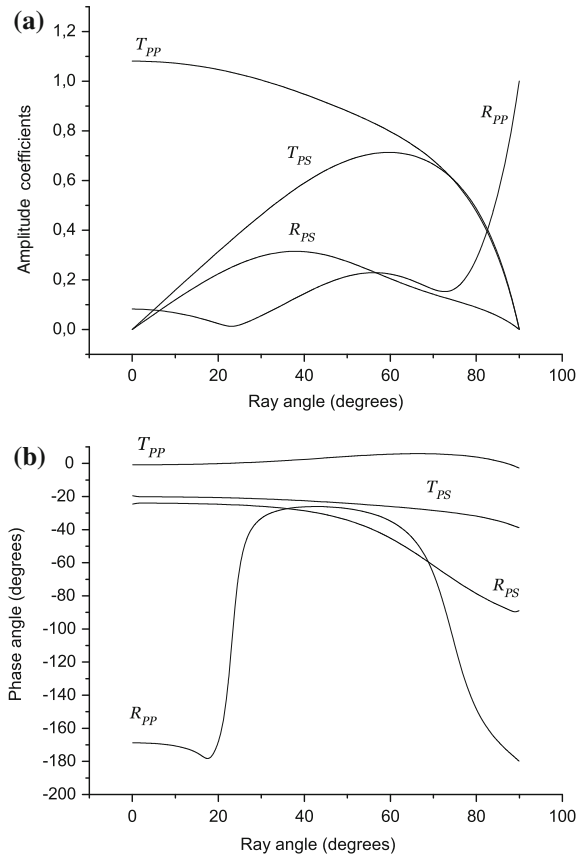


Figure 11

Reflection and transmission coefficients for a single interface as a function of the ray angle. The incident wave is compressional (P) and its frequency is 3 Hz

$$p_{11} = (70, 9) \text{ GPa}$$

$$p_{12} = (68, -5) \text{ GPa}$$

$$p_{13} = (73, -2) \text{ GPa}$$

$$p_{33} = (80, 6) \text{ GPa}$$

$$p_{55} = (1, 6) \text{ GPa}$$

$$p_{66} = (1, 7) \text{ GPa},$$

corresponding to 700 °C. The frequency is 3 Hz. The following figures display the absolute values of the scattering coefficients and their respective phases. Figures 11 and 12 show the reflection and transmission coefficients as a function of the ray angle, corresponding to incident P- and S-waves, respectively. The

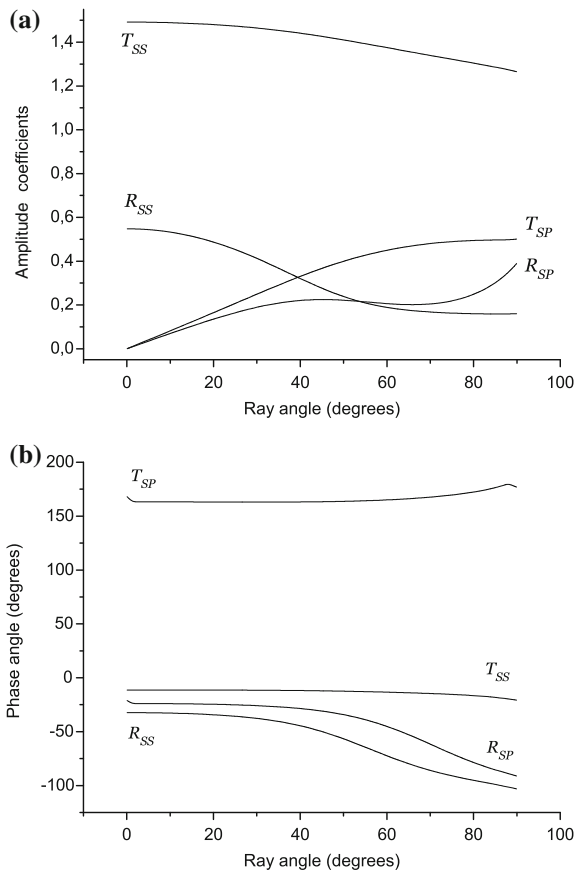


Figure 12

Reflection and transmission coefficients for a single interface as a function of the ray angle. The incident wave is shear (S) and its frequency is 3 Hz

PP reflection coefficient has an elastic Brewster angle (CARCIONE, 2007) approximately at $\theta_B = 23^\circ$, where a phase change occurs (the coefficient changes sign). Here we define the Brewster angle as the incidence angle for which the reflection coefficient is zero. Actually, the real part of R_{PP} is negative at near offset and becomes positive beyond θ_B . This real part changes sign and becomes negative again at 72° . There is substantial conversion from P to S with a maximum value at nearly 40° . On the other hand, R_{SS} (see Fig. 12) is high (0.55) at near offsets, since the S-velocity contrast at the interface is higher than the P-velocity contrast. The real part of this coefficient is positive as a function of the ray angle.

Next, we consider a ductile layer (slab) embedded in an isotropic crust with plane-wave moduli p_{33} and p_{55} . The ductile medium is anisotropic with the

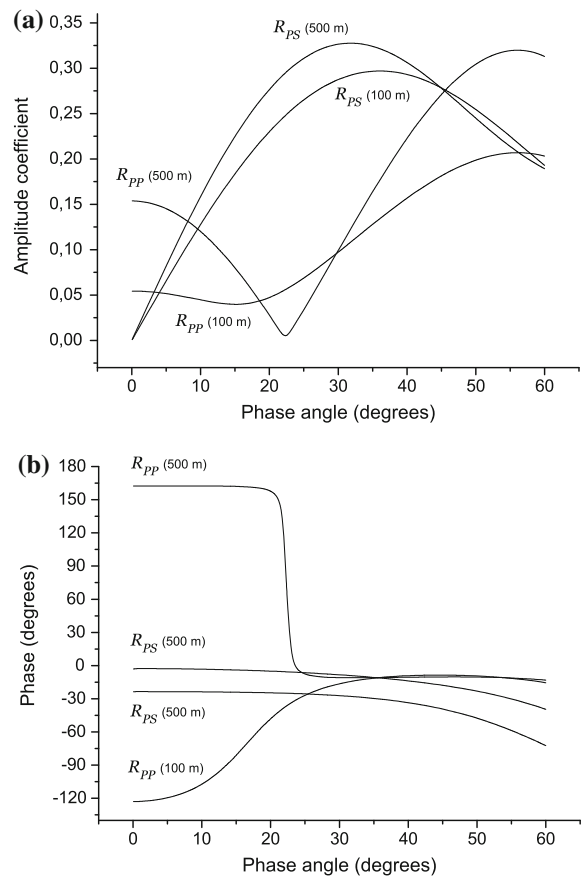


Figure 13

Reflection and transmission coefficients for a ductile layer as a function of the incidence phase angle. The thickness of the layer is indicated. The incident wave is compressional (P) and its frequency is 3 Hz

properties indicated above. Figure 13 and 14 show the reflection and transmission coefficients as a function of the incidence phase angle, corresponding to incident P- and S-waves, respectively. The normal-incidence reflection coefficient increases with the slab thickness and a Brewster angle is clear at $\theta_B = 22^\circ$ for a slab thickness of 0.5 km, as in the case of a single interface. This effect is more pronounced for a thicker slab, as can be seen from the steep phase change in Fig. 11b. The converted P to S wave has a high amplitude at intermediate angles, around 30° . On the other hand, R_{SS} and R_{SP} decrease with the incidence angle but are not much sensitive to the slab thickness.

Finally, we compute seismograms in a homogeneous medium by using Eq. (17). P- and S-wave synthetic pulses as a function of temperature are shown

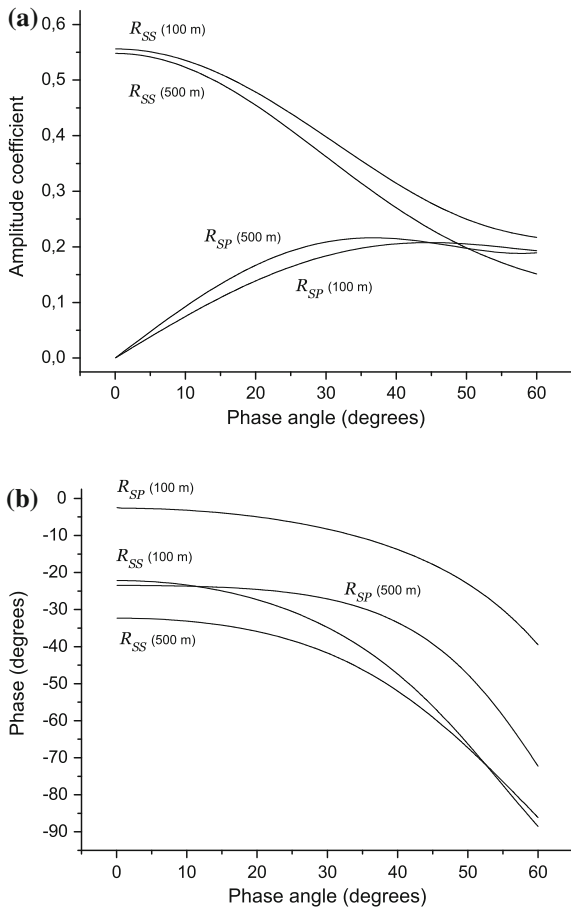


Figure 14

Reflection and transmission coefficients for a ductile layer as a function of the incidence phase angle. The thickness of the layer is indicated. The incident wave is shear (S) and its frequency is 3 Hz

in Figs. 15 and 16, respectively. The source is a Hanning pulse in the bandwidth range 5–60 Hz (OPPENHEIM and SCHAFER, 1975). High attenuation is observed in the highly dispersive zone at the critical temperature of 718 °C. As expected, S waves show also high attenuation at high temperatures and do not propagate.

7. Conclusions

The abrupt brittle–plastic transition is believed to be the lower limit of seismicity and may be an indication of geothermal activity, since its reflectivity may reveal the presence of partial melting and/or overpressured fluids. Combining a Burgers mechanical kernel and the Arrhenius equation to calculate the flow viscosity, we

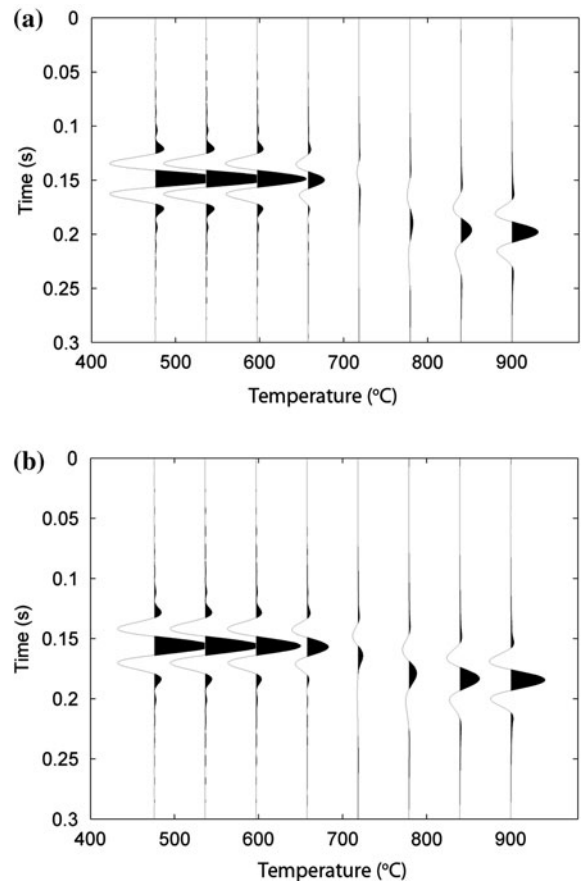


Figure 15

P-wave seismograms at different temperatures, corresponding to the 11 (a) and 33 (b) components. The source is a Hanning pulse in the bandwidth range 5–60 Hz

obtain a realistic rheological model describing the transition. The model includes anisotropy and seismic wave attenuation. The P-wave velocities decrease after a given viscosity related to a critical (transition) temperature and the P-wave attenuation has a maximum at this transition, where the quality factors have a minimum value, which depends only on the elastic properties of the medium. This occurs at a critical viscosity which is inversely proportional to the frequency. At higher temperatures the medium becomes an anisotropic fluid. This is consistent with the fact that a pure solid and a pure liquid have weak attenuation and partial saturation (melting in this case) shows lower attenuation. In the ductile regime, the shear-wave quality factor approaches zero and the P-wave attenuation anisotropy is more pronounced.

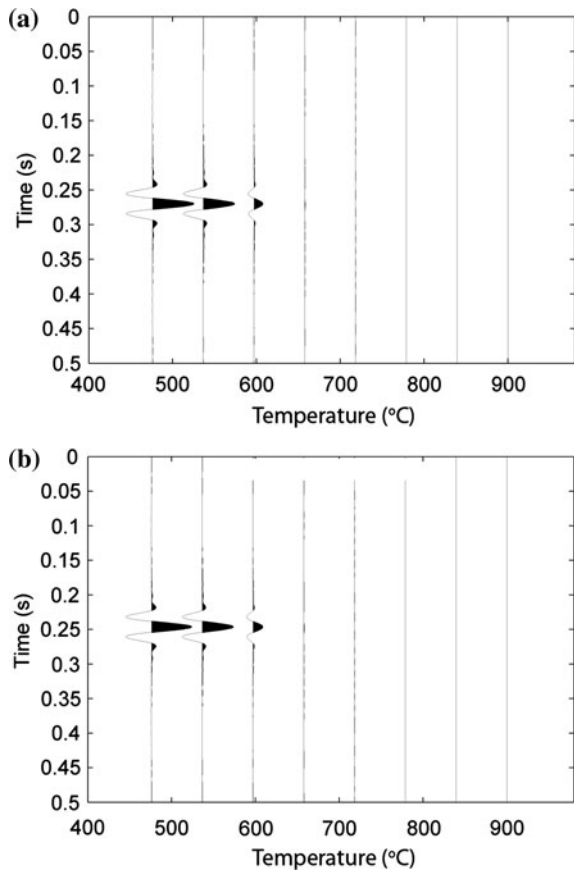


Figure 16

S-wave seismograms at different temperatures, corresponding to the 55 (a) and 66 (b) components. The source is a Hanning pulse in the bandwidth range 5–60 Hz

Regarding a sharp brittle–ductile interface, the PP reflection coefficient has a Brewster angle and there is substantial conversion from P to S energy. The SS coefficient is high at near offsets since the S-velocity contrast at the interface is higher than the P-velocity contrast. On the other hand, for a ductile layer (slab) embedded in an isotropic crust, the normal-incidence reflection coefficient increases with the slab thickness and a Brewster angle is clear for a thick slab. The SS and SP reflection coefficients decrease with the incidence angle but are not much sensitive to the slab thickness. Finally, P-wave synthetic pulses show high attenuation and dispersion at the critical temperature, where partial melt occurs, and can be used as an indication of the presence of the brittle–ductile transition.

Appendix

Wave Velocities and Quality Factors

The complex velocities are required to calculate wave velocities and quality factors of the fractured medium. They are given by

$$\begin{aligned}
 v_{qP} &= (2\rho)^{-1/2} \sqrt{p_{11}l_1^2 + p_{33}l_3^2 + p_{55} + A} \\
 v_{qSV} &= (2\rho)^{-1/2} \sqrt{p_{11}l_1^2 + p_{33}l_3^2 + p_{55} - A} \\
 v_{SH} &= \rho^{-1/2} \sqrt{p_{66}l_1^2 + p_{55}l_3^2} \\
 A &= \sqrt{[(p_{11} - p_{55})l_1^2 + (p_{55} - p_{33})l_3^2]^2 + 4[(p_{13} + p_{55})l_1l_3]^2}
 \end{aligned} \tag{25}$$

(CARCIONE, 2007), where $l_1 = \sin \theta$ and $l_3 = \cos \theta$ are the directions cosines, θ is the propagation angle between the wavenumber vector and the symmetry axis, and the three velocities correspond to the qP, qS and SH waves, respectively. The phase velocity is given by

$$v_p = \left[\text{Re} \left(\frac{1}{v} \right) \right]^{-1}, \tag{26}$$

where v represents either v_{qP} , v_{qSV} or v_{SH} . The energy-velocity vector of the qP and qSV waves is given by

$$\frac{\mathbf{v}_e}{v_p} = (l_1 + l_3 \cot \psi)^{-1} \hat{\mathbf{e}}_1 + (l_1 \tan \psi + l_3)^{-1} \hat{\mathbf{e}}_3 \tag{27}$$

(CARCIONE, 2007), where

$$\tan \psi = \frac{\text{Re}(\beta^* X + \xi^* W)}{\text{Re}(\beta^* W + \xi^* Z)}, \tag{28}$$

defines the angle between the energy-velocity vector and the z -axis (the ray angle), the asterisk denotes complex conjugate,

$$\begin{aligned}
 \beta &= \sqrt{A \pm B}, \\
 \xi &= \pm p v \sqrt{A \mp B}, \\
 B &= p_{11}l_1^2 - p_{33}l_3^2 + p_{55} \cos 2\theta,
 \end{aligned} \tag{29}$$

where the upper and lower signs correspond to the qP and qS waves, respectively. Moreover,

$$\begin{aligned}
 W &= p_{55}(\xi l_1 + \beta l_3), \\
 X &= \beta p_{11}l_1 + \xi p_{13}l_3, \\
 Z &= \beta p_{13}l_1 + \xi p_{33}l_3
 \end{aligned} \tag{30}$$

(CARCIONE, 2007), where “pv” denotes the principal value, which has to be chosen according to established criteria (SIDLER *et al.*, 2008).

On the other hand, the energy velocity of the SH wave is

$$\mathbf{v}_e = \frac{v_p}{\rho \operatorname{Re}(v)} \left[I_1 \operatorname{Re} \left(\frac{p_{66}}{v} \right) \hat{\mathbf{e}}_1 + I_3 \operatorname{Re} \left(\frac{p_{55}}{v} \right) \hat{\mathbf{e}}_3 \right]. \quad (31)$$

Finally, the quality factor is given by

$$Q = \frac{\operatorname{Re}(v^2)}{\operatorname{Im}(v^2)}. \quad (32)$$

REFERENCES

- ANDERSON, D. L. (1989). *Theory of the Earth*. Boston: Blackwell Scientific Publications.
- BATINI, F., and NICOLICH, R. (1985). *P and S reflection seismic profiling and well logging in the Travale geothermal field*. *Geothermics* 14, 731–747.
- BROGI, A., LAZZAROTTO, A., LIOTTA, D., and RANALLI, G. (2003). *Extensional shear zones as imaged by reflection seismic lines: the Larderello geothermal field (central Italy)*. *Tectonophysics*, 363, 127–139.
- CAMELI, G. M., DINI, I. and LIOTTA, D. (1993). *Upper crustal structure of the Larderello geothermal as a feature of post collisional extensional tectonics (Southern Tuscany, Italy)*. *Tectonophysics*, 224, 413–423.
- CARCIONE, J. M. (1997). *Reflection and transmission of qP-qS plane waves at a plane boundary between viscoelastic transversely isotropic media*. *Geophys. J. Internat.* 129, 669–680.
- CARCIONE, J. M. (2007). *Wave fields in real media: Wave propagation in anisotropic, anelastic, porous and electromagnetic media*. *Handbook of Geophysical Exploration*, vol. 38, Elsevier (2nd edition, revised and extended).
- CARCIONE, J. M., and CAVALLINI, F. (1994). *A rheological model for anelastic anisotropic media with applications to seismic wave propagation*. *Geophys. J. Int.* 119, 338–348.
- CARCIONE, J. M., and CAVALLINI, F. (2002). *Poisson's ratio at high pore pressure*. *Geophys. Prosp.* 50, 97–106.
- CARCIONE, J. M., FINETTI, I., and GEI, D. (2003). *Seismic modeling study of the Earth's deep crust*. *Geophysics* 68, 656–664.
- CARCIONE, J. M., HELLE, H. B., and GANGI, A. F. (2006). *Theory of borehole stability when drilling through salt formations*. *Geophysics* 71, F31–F47.
- CARCIONE, J. M., and PICOTTI, S. (2006). *P-wave seismic attenuation by slow-wave diffusion. Effects of inhomogeneous rock properties*. *Geophysics*, 71, O1–O8.
- CARTER, N. L., and HANSEN, F. D. (1983). *Creep of rocksalt*. *Tectonophysics* 92, 275–333.
- CARTER, N., and S. KIRBY (1978). *Transient creep and semibrittle behaviour of crystalline rock*. *Pure Appl. Geophys.* 116, 807–839.
- CASTRO, R. R., GALLIPIOLI, M. R., and MUCCIARELLI, M. (2008). *Crustal Q in southern Italy determined from regional earthquakes*. *Tectonophysics* 457(2), 96–101.
- CHAUVEAU, B. and KAMINSKI, E. (2008). *Porous compaction in transient creep regime and implications for melt, petroleum, and CO2 circulation*. *J. Geophys. Res.* 113, B09406.
- CHEN, J., TENG, J., and BADAL, J. (2009). *Constraining the anisotropy structure of the crust by joint inversion of seismic reflection travel times and wave polarizations*. *J. Seismol.* 13, 219–240.
- DE MATTEIS, R., VANORIO, T., ZOLLO, A., CIUFFI, S., FIORDELISI, A., and SPINELLI, E. (2008). *Three-dimensional tomography and rock properties of the Larderello-Travale geothermal area, Italy*. *Physics of the Earth and Planetary Interiors*, doi:10.1016/j.pepi.2008.04.019
- DOGLIONI, C., BARBA, S., CARMINATI, E., and RIGUZZI, F. (2011). *Role of the brittle–ductile transition on fault activation*. *Phys. Earth Planet. Inter.* 184, 160–171.
- DRAGONI, M. (1990). *Stress relaxation at the lower dislocation edge of great shallow earthquakes*, *Tectonophysics* 179, 113–119.
- DRAGONI, M. and PONDRELLI, S. (1991). *Depth of the brittle–ductile transition in a transcurrent boundary zone*. *Pure and Applied Geophysics* 135, 447–461
- ENGELDER, T. (1993). *Stress regimes in the lithosphere*, Princeton University Press.
- GANGI, A.F. (1981). *A constitutive equation for one-dimensional transient and steady-state flow of solids*. *Mechanical Behavior of Crustal Rocks*, *Geophysical Monograph* 24, AGU, 275–285.
- GANGI, A. F., 1983, *Transient and steady-state deformation of synthetic rocksalt*. *Tectonophysics* 91, 137–156.
- HEGRET, G. (1987). *Stress assumption for underground excavation in the Canadian Shield*, *Int. J. Rock Mech. Min. Sci. Geomech. Abstr.* 24, 95–97.
- HOBBS, B. E., *et al.* (1986). *Earthquakes in the ductile regime*. *Pure and Applied Geophysics* 124, 310–336.
- KAMPFMANN, W. and BERCKHEMER, H. (1985). *High temperature experiments on the elastic and anelastic behaviour of magmatic rocks*. *Phys. Earth Planet. Interiors* 40, 223–247.
- KIRBY, S. H. and KRONENBERG, A. K. (1987). *Rheology of the lithosphere: selected topics*, *Rev. Geophys. and Space Phys.* 25, 1219–1244.
- LIOTTA, D., and RANALLI, G. (1999). *Correlation between seismic reflectivity and rheology in extended lithosphere: southern Tuscany, Inner Northern Apennines, Italy*. *Tectonophysics* 315, 109–122.
- MAINARDI, F. (2010). *Fractional Calculus and Waves in Linear Viscoelasticity*, Imperial College Press, London.
- MAINARDI, F., and SPADA, G. (2011). *Creep, relaxation and viscosity properties for basic fractional models in rheology*. *The European Physical Journal, Special Topics* 193, 133–160.
- MATSUMOTO, S., and HASEGAWA, A. (1996). *Distinct S-wave reflector in the midcrust beneath Nikko-Shirane volcano in the northeastern Japan arc*. *J. Geophys. Res.* 101(B2), 3067–3083.
- MEISSNER, R., and STREHLAU, J. (1982). *Limits of stresses in continental crusts and their relation to the depth-frequency distribution of shallow earthquakes*. *Tectonics* 1, 73–89.
- OPPENHEIM, A. V., and SCHAFER, R. W., (1975). *Digital signal processing*. Prentice-Hall, Englewood Cliffs, New York.
- POLETTI, F., CORUBOLO, P., SCHLEIFER, A., FARINA, B. M., POLLARD, J., and GROZDANICH, B. (2011). *Seismic while drilling for geophysical exploration in geothermal wells*, *GRC Transactions*, Vol. 35, 1737–1741.
- POLETTI, F., and MIRANDA, F. (2004). *Seismic while drilling. Fundamentals of drill-bit seismic for exploration*, Elsevier Science, Amsterdam.

- RUTTER, E. H., (1986). *On the nomenclature of mode of failure transitions in rocks*. *Tectonophysics* 122, 381–387.
- SATO, H. (2005). *Rock anelasticity studies at high pressure and temperature*. *Journal of Geography* 114, 1022–1031.
- SATO, H., SACKS, S., MURASE, T., MUNCILL, G., and FUKUYAMA, H. (1988). Attenuation of compressional waves in peridotite measured as a function of temperature at 200 MPa. *PAGEOPH* 128, 433–447.
- SIDLER, R., CARCIONE, J. M., and HOLLIGER, K. (2008). *On the evaluation of the plane-wave reflection coefficients in anelastic media*. *Geophys. J. Internat.* 175, 94–102.
- SINGH, S. C., TAYLOR, M. A. J., and MONTAGNER, J. P. (2000). On the presence of liquid in Earth's inner core. *Science* 287, March Issue.
- SPETZLER, H. and ANDERSON, D. L. (1968). *The effect of temperature and partial melting on velocity and attenuation in a simple binary system*. *J. Geophys. Res.* 73, 6051–6060.
- THOMSON, W. T. (1950). *Transmission of elastic waves through a stratified solid material*. *J. Appl. Phys.* 21, 89–93.
- VAVRYČUK, V. (2005). *Focal mechanisms in anisotropic media*. *Geophys. J. Int.* 161, 334–346.
- VERGNOLLE, M., POLLITZ, F., and CALAIS, E. (2003). *Constraints on the viscosity of the continental crust and mantle from GPS measurements and postseismic deformation models in western Mongolia*. *J. Geophys. Res.* 108, B10, 2502, doi:[10.1029/2002JB002374](https://doi.org/10.1029/2002JB002374), 2003
- WALSH J. B. (1969). *A new analysis of attenuation in partially melted rock*. *J. Geophys. Res.* 74, 4333–4337.

(Received October 20, 2012, revised January 8, 2013, accepted January 11, 2013, Published online February 7, 2013)